Supporting information for:

Stabilizing zinc anodes via engineering active sites and pore structure of functional composite layers

Kun Li et al.

The file includes:

Part I. Supplementary Notes

Note S1. Nernst-Planck equation (Equation S1):

$$J_d = Cv_x - D(^{dC}/_{dx}) - (^{qCD}/_{kT})(^{dV}/_{dx}) \quad \text{(S1)}$$

The mass transfer process of Zn^{2+} can be explained by the Nernst-Planck equation (**Equation S1**), where v_x represents the convective velocity, C stands for the concentration, x is the distance, D is the diffusion coefficient, V is the potential, q means unit charge, k is the Boltzmann's constant, T stands for the temperature, and J_d is the diffusion flux. According to the equation, the electrochemical reaction process of Zn at the anode is influenced by three factors: convection velocity (v_x), concentration gradient (dC/dx), and potential concentration (dV/dx). Most of these factors are related to water molecules and solvated shells. Furthermore, concentration polarization of the electrolyte, perturbations caused by the escape of gases from the hydrogen evolution reaction (HER), and temperature fluctuations all affect the growth of dendrites.

Note S2. Methods

Material synthesis. The copper foil (purity of 99.99%, thickness of 9 μm), stainless steel sheet and zinc foil (purity of 99.99%, thickness of 80 μm) were bought by Tianjin Iweixin Chemical Technology and Shenzhen Kejing Star Technology. $ZnSO_4 \cdot 7H_2O$ (AR, 99.5%), N, N-dimethylformamide (DMF) (AR, 99%), N-methyl-2-pyrrolidone (NMP) (AR, 99%) and triethylamine were bought by Chengdu Kelong Chemical Reagent Factory. The active carbon (YP-50F, 99.3%) was bought by Guangdong Canrd New Energy Technology Co., Ltd. Polyvinylidene fluoride (PVDF) was bought by French Arkema Co., Ltd. Zirconium tetrachloride (AR, 98%) was bought by Shanghai

Aladdin Biochemical Technology Co., Ltd. 2-amino-terephthalic acid was bought by Shanghai Maclin Biochemical Technology Co., Ltd. Glacial acetic acid was bought by Chengdu Jinshan Reagent Co., Ltd. And button battery (CR2032) cases are bought from Tianjin Anohe New Energy Technology Co., Ltd. All experiments were carried out strictly in standard procedures and repeated for more than three times to avoid accidental errors.

***Preparation of FCL@Zn*.** Firstly, 1.09 g of 2-amino-terephthalic acid was dissolved in 60 mL of DMF solution, then 0.1 mL of triethylamine solution was added, and the mixture was continuously stirred for 30 minutes. Then add 20 mL of glacial acetic acid solution to the above solution, reseal and stir for 30 minutes until evenly mixed. The mixture, named solution A, was transferred to a 250 mL round-bottomed flask and heated in an oil bath to 120 ℃. 1.4 g zirconium tetrachloride was dissolved in 40 mL of DMF solution, sealed and stirred for 10 minutes, and the resulting solution was named solution B. When the temperature of the round-bottom flask in the oil bath reaches 120 ℃, the B solution is slowly added to the A solution, and the temperature is kept at 120 ℃ for 6 hours, and finally the brown precipitate is obtained. The brown precipitates were centrifuged and washed three times with 50 mL of DMF and methanol respectively and dried in a 70 ℃ oven for 12 hours under vacuum. Finally, *FCL* material powder was obtained.

PVDF and FCL in a mass ratio of 1.5: 9 were added to NMP solvent and stirred 12h. The resulting slurry was then applied to the pre-cleaned bare zinc foil by the doctor blade method and vacuum dried for 6 hours. The FCL@Zn foil was then perforated into

a 16 mm diameter electrode for further use.

***Materials characterization*.** We used the X-ray diffraction to analyze the crystal phase of the material (XRD, D/MAX-IIIC). Thermo Scientific K-Alpha$^+$ X-ray photoelectron spectrometer (XPS) was used to characterize the surface chemical state and composition of the samples. The surface morphology and elemental composition of the materials were characterized by scanning electron microscopy (SEM) and energy spectrometry (EDS) (Zeiss Gemini SEM 300) (Smartedx). Fourier transform infrared (FTIR) spectroscopy and Raman spectroscopy are used to detect the bonding state of the surface of the prepared sample, analyze the composition and lattice distortion and other information. At the same time, in situ Raman spectroscopy was used to study the effective control of interface disturbance and other microscopic factors in electroplating/stripping state. And we used Micromeritics ASAP 2460 to determine the nitrogen adsorption-desorption isotherms of the materials.

***Computational details*.** The spin-polarized density functional theory (DFT) calculations were carried out in the Vienna ab initio simulation package (VASP) based on the plane-wave basis sets with the projector augmented-wave method. The exchange-correlation potential was treated by using a generalized gradient approximation (GGA) with the Perdew-Burke-Ernzerhof (PBE) parametrization. The energy cutoff was set to be 500 eV. The Brillouin-zone integration was sampled with a Γ-centered Monkhorst-Pack mesh of 2 × 2 × 1 by VASPKIT. The structures were fully relaxed until the maximum force on each atom was less than 0.05 eV/Å, and the energy convergent standard was 10^{-5} eV. The van der Waals correction of Grimme's DFT-D3

model was also adopted. The Binding energies (E_b) were calculated as Eb= E_{AB} -E_A - E_B, where E_{AB}, E_A, and E_B, are the total energies of the optimized total system, the FCL, and the Zn, respectively.

Finite element simulations. A simplified 2D model was established to simulate the process of ion deposition based on COMSOL. The domain of the entire model was set to 100×80 μm^2. The dendritic crystal of Zn electrode surface was represented by an interpolation curve with a width of 5 μm, and the FCL layer was constructed as the similar way. Furthermore, the initial electrolyte concentration was set as 2000 mol m^{-3} and the ionic conductivity was about 5 S m^{-1}.

Preparation of active carbon cathode. Commercial active carbon powder was used as the cathode active material. In particular, a uniformly mixed slurry of active carbon powder, Super P, and PVDF (7:2:1) in NMP was molded on a stainless-steel foil and dried overnight in a vacuum oven at 60 ℃. The AC cathode payload mass was about 5 mg cm^{-2}.

Electrochemical measurements. The effect of FCL on the electrochemical behavior of zinc anodes and full cells was performed using Zn||Cu symmetric cells, Zn||Zn symmetric cells, and Zn||AC hybrid supercapacitors in a systematic way. Unless otherwise stated, the thickness of the zinc anode utilized in this paper was 0.08 mm. The cells were fabricated into CR2032 coin cells using 2M $ZnSO_4$ aqueous electrolyte and glass fiber paper as spacers. Coulombic efficiency (CE) and Galvanostatic charge-discharge (GCD) were measured on LAND battery test system (CT2001A, China). The reversibility of the plating/stripping process about zinc ions was determined using a

Zn||Cu half-cells for CE testing. GCD measurements for Zn||Zn symmetric cells using two FCL@Zn as positive and negative electrodes. The cycle stability and cycle life of zinc anode were tested at constant current density and areal capacity. The rate performance and nucleation over potential were also tested by LAND battery test system (CT2001A).

Cyclic voltammetry (CV), Electrochemical impedance spectroscopy (EIS) and Chronoamperometry (CA) were conducted on Bio-Logic SP-150 electrochemical workstation. More specifically, the EIS has an amplitude of 10 mV and a frequency range from 10^5 Hz to 10^{-1} Hz. The external voltage polarization is set to 150 mV for testing 3D diffusion.

Zn^{2+} deposition barrier could be quantitatively evaluated based on the temperature-dependent EIS, according to the following equation:

$$\ln\left(Rct^{-1}\right) = lnA - {}^{E_a}/_{RT} \quad \text{(Equation 2)}$$

Where T is the absolute temperature, R is the gas constant, A is the pre-exponential factor, E_a is the activation energy and R_{ct} is the interfacial Zn^{2+} transfer resistance.

Corrosion current and corrosion potential of linear polarization curve were tested on electrochemical workstation (CHI760E) in the three-electrode system in which Ti foil, Zn foil, Ag/AgCl were employed as counter, working and reference electrodes, respectively. To elucidate the effect of the FCL layer on hydrogen evolution, the HER of the zinc anode with and without the FCL layer added to the 2M $ZnSO_4$ aqueous electrolyte was investigated by linear scanning voltammetry (LSV). The scan rate of LSV measurement was 5 mV s^{-1} in a two-electrode system, where Zn foil with or

without FCL and stainless-steel plate were used as counter /reference and working electrodes, respectively. Corresponding electrochemistry experiments were repeated for more than three times.

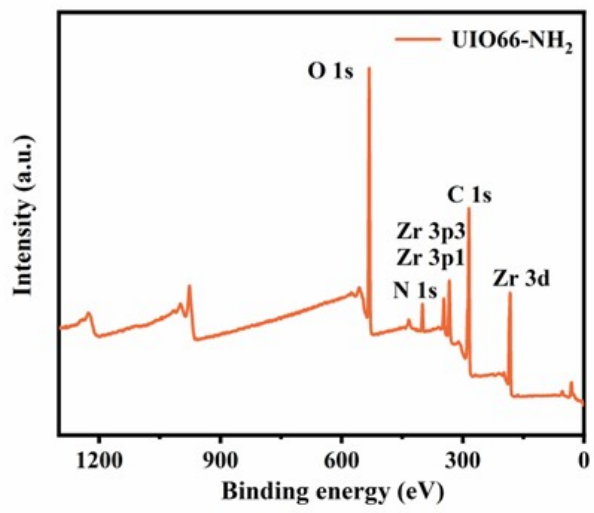

Fig. S1 The broad XPS spectrum of the materials.

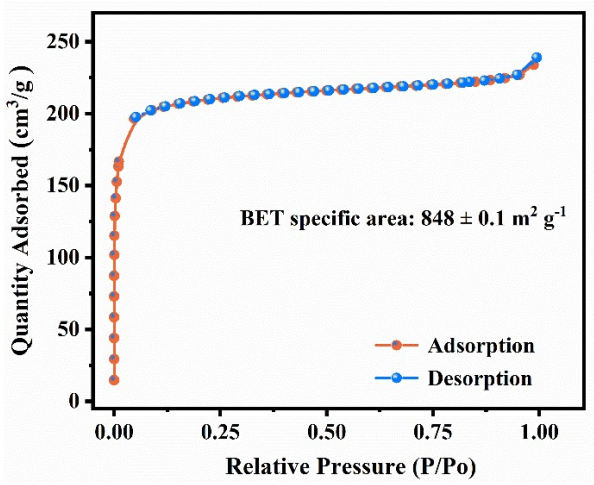

Fig. S2 N_2 adsorption-desorption curves of the sample particles. The BET specific area was repeated three times, and the average value was obtained

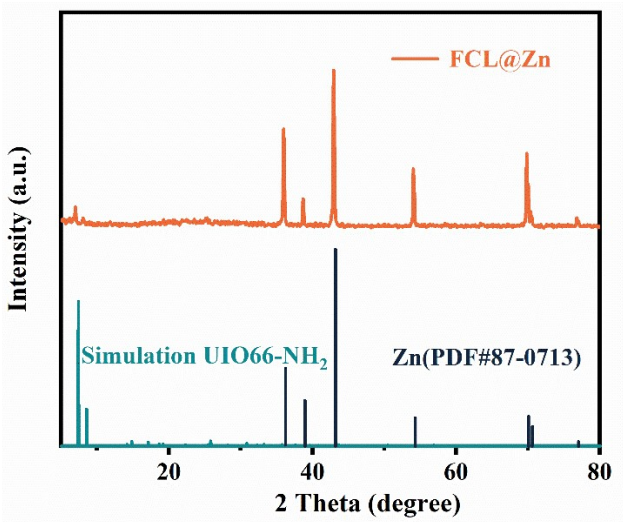

Fig. S3 XRD spectra of FCL@Zn.

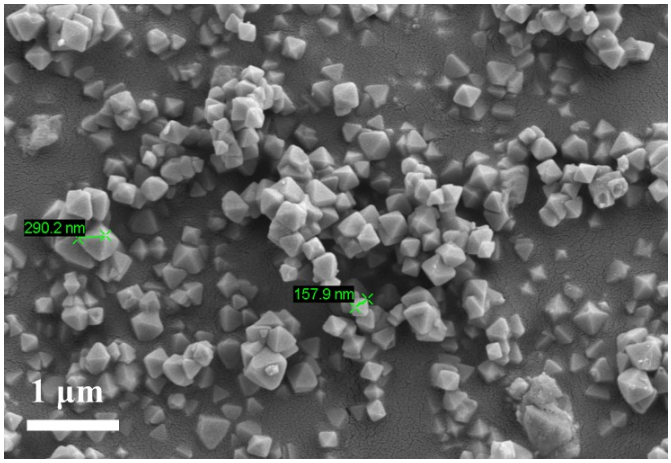

Fig. S4 The SEM enlarged image of the sample powder.

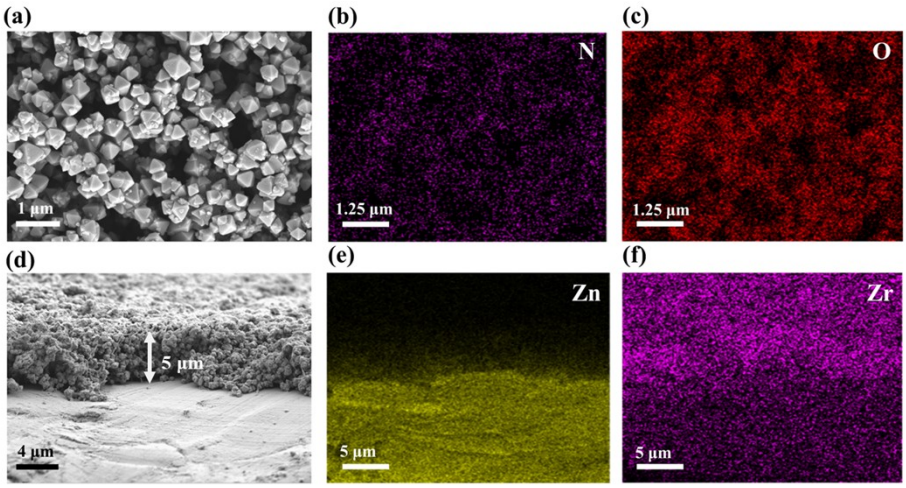

Fig. S5 (a) The SEM enlarged image of the FCL@Zn. (b)(c) The element mapping of the FCL@Zn. (d) The cross-section SEM image of the FCL@Zn. (e)(f) The element mapping of the cross-section of the FCL@Zn.

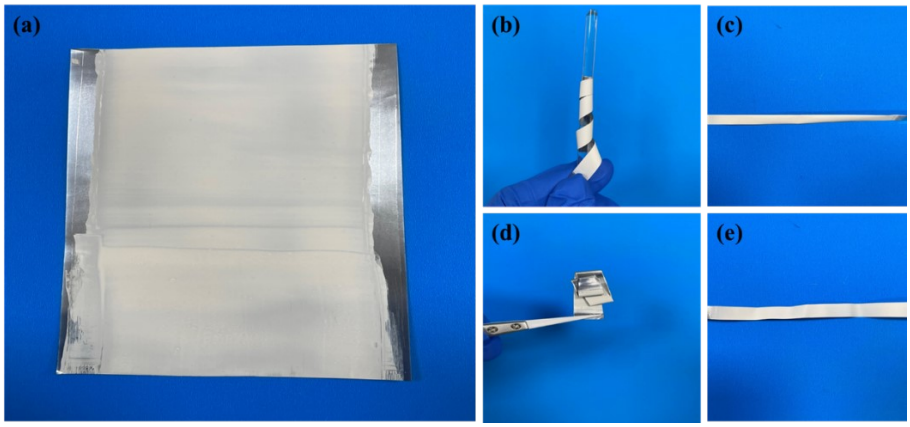

Fig. S6 (a) Optical photographs of FCL@Zn. (b)(c) Optical photographs of FCL@Zn mechanical property test torsion test. (d)(e) Optical photographs of FCL@Zn mechanical property test folding test.

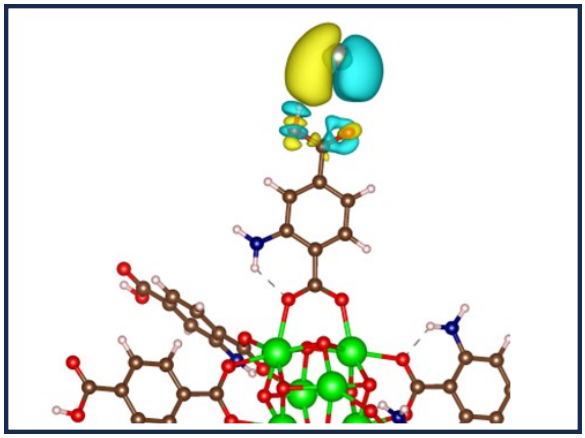

Fig. S7 Charge density differences of the O sites in the FCL with Zn^{2+} adsorption. Yellow means the charge accumulates, cyan means the charge dissipates.

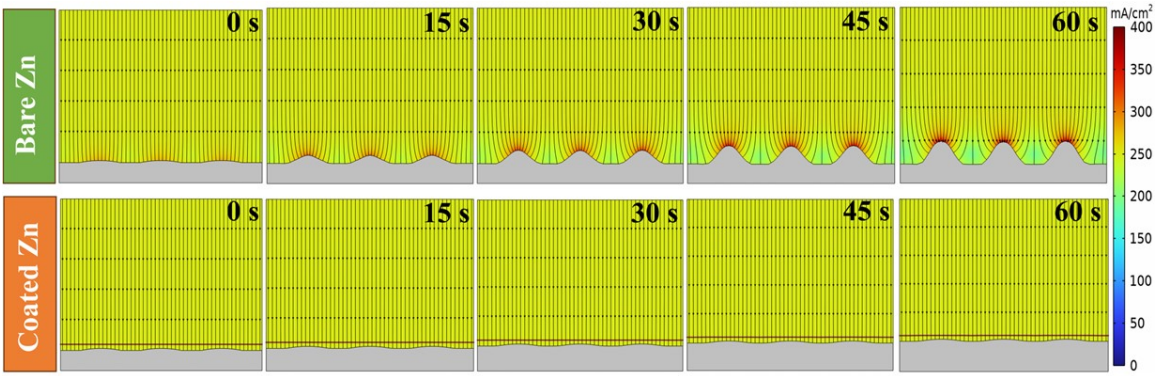

Fig. S8 FES of the local current density distribution at the electrode interface from t=0 s to t=60 s.

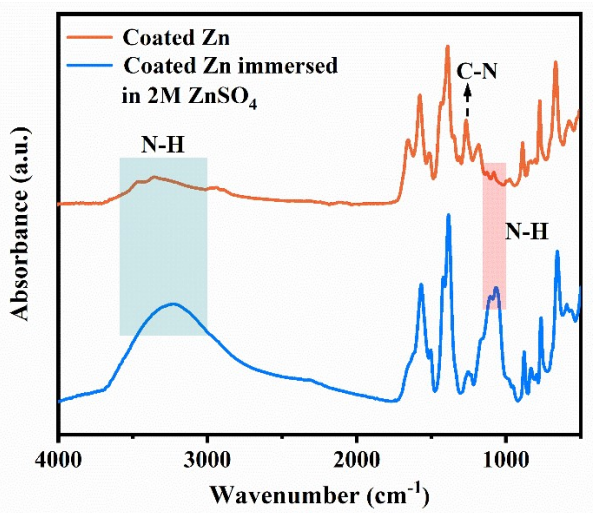

Fig. S9 FTIR spectra of FCL@Zn electrode before/after electrolyte immersion.

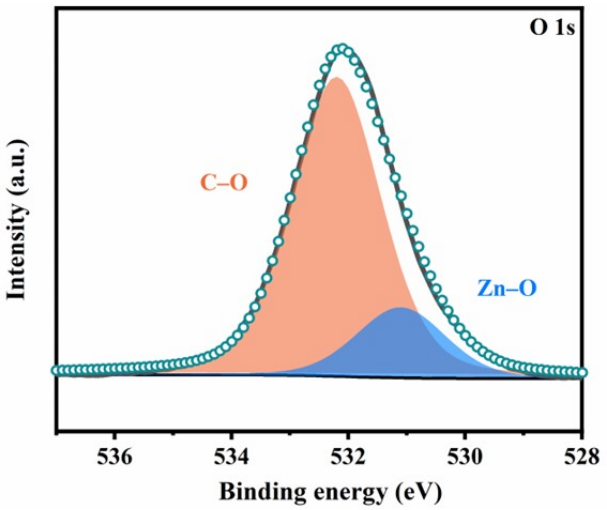

Fig. S10 O 1s XPS spectra of FCL@Zn electrodes after immersion in the electrolyte.

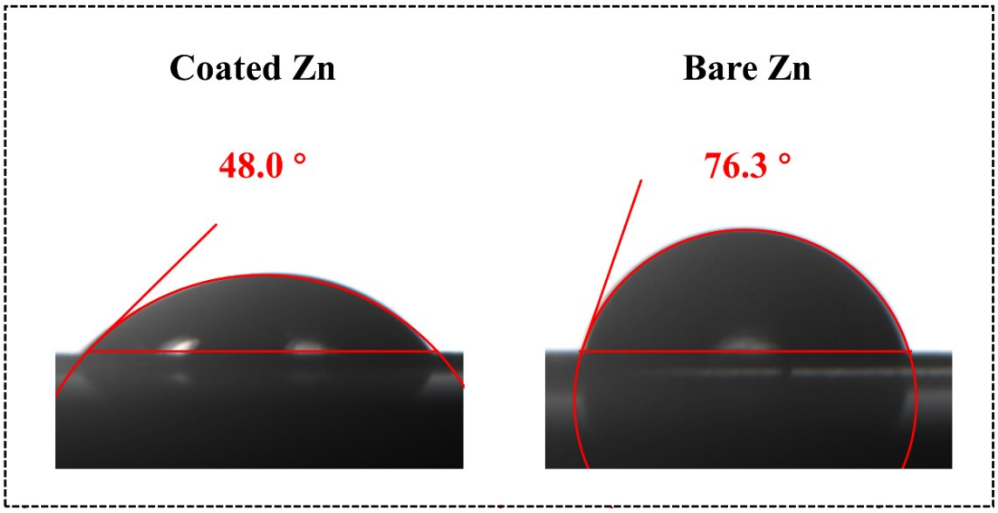

Fig. S11 Contact angle test (a) FCL@Zn; (b) Bare Zn foil.

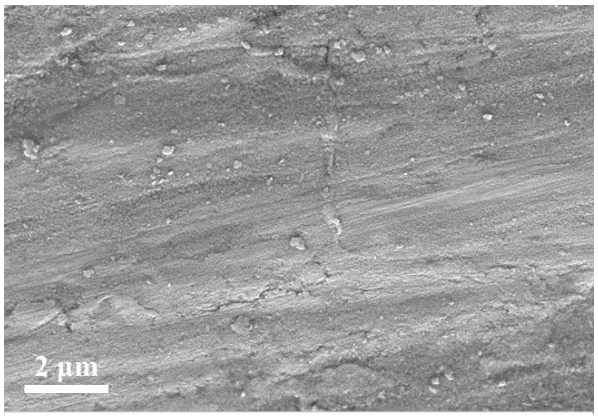

Fig. S12 SEM image of bare Zn foil before cycling.

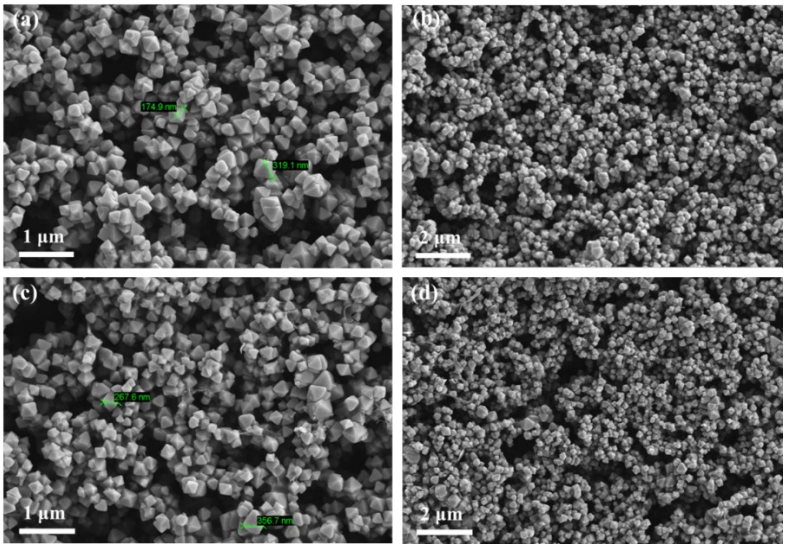

Fig. S13 (a) (b) SEM morphology of artificial layer before cycling; (c) (d) SEM morphology of artificial layer after cycling.

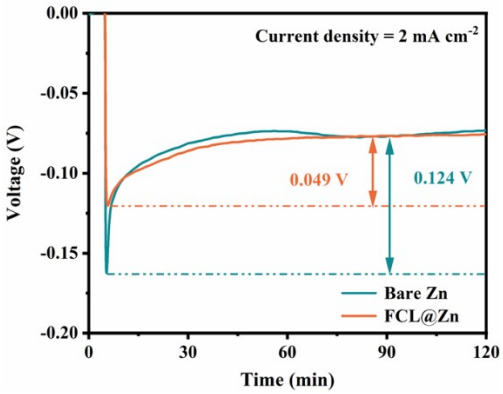

Fig. S14 Nucleation overpotential curves for FCL@Zn and bare Zn foil.

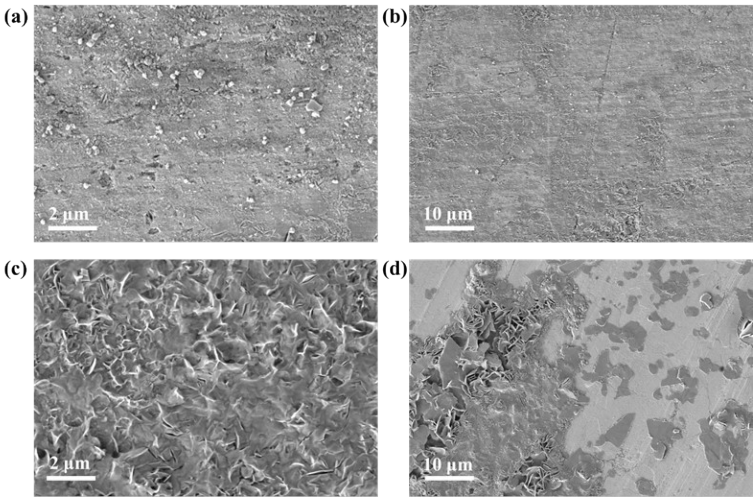

Fig. S15 SEM images of (a) (b) FCL@Zn and (c) (d) bare Zn foil after 3 days of immersion.

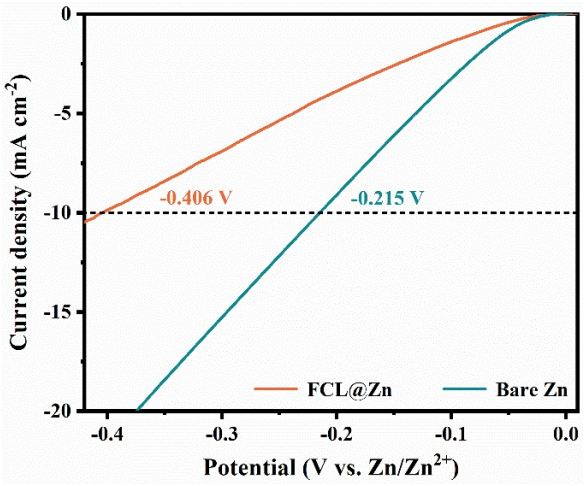

Fig. S16 LSV curve of FCL@Zn and bare Zn.

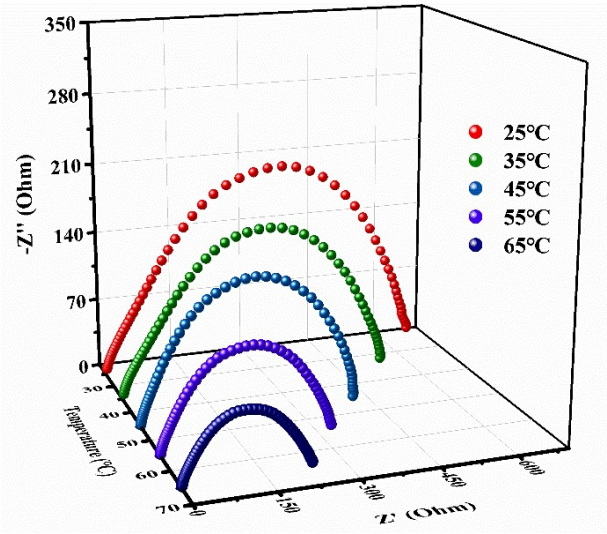

Fig. S17 EIS raw data of bare Zn.

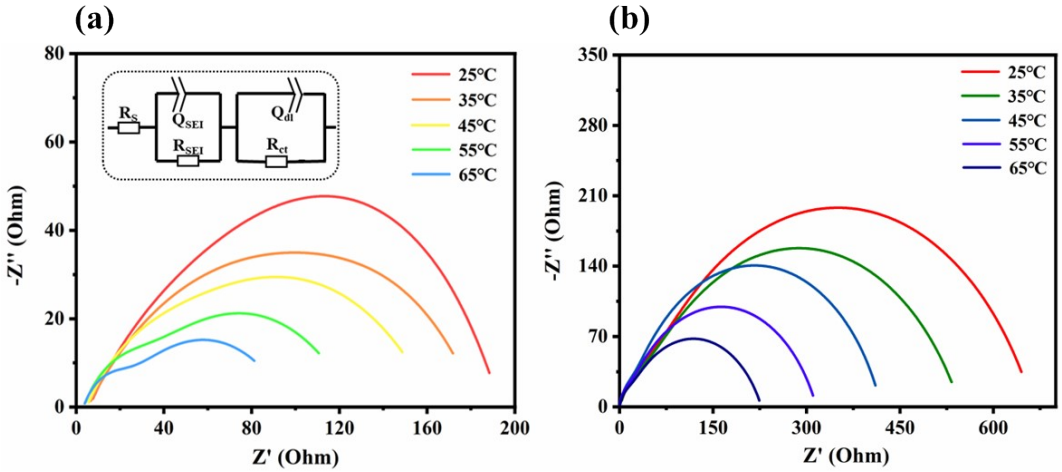

Fig. S18 EIS fitting curve (a) FCL@Zn and (b) bare Zn.

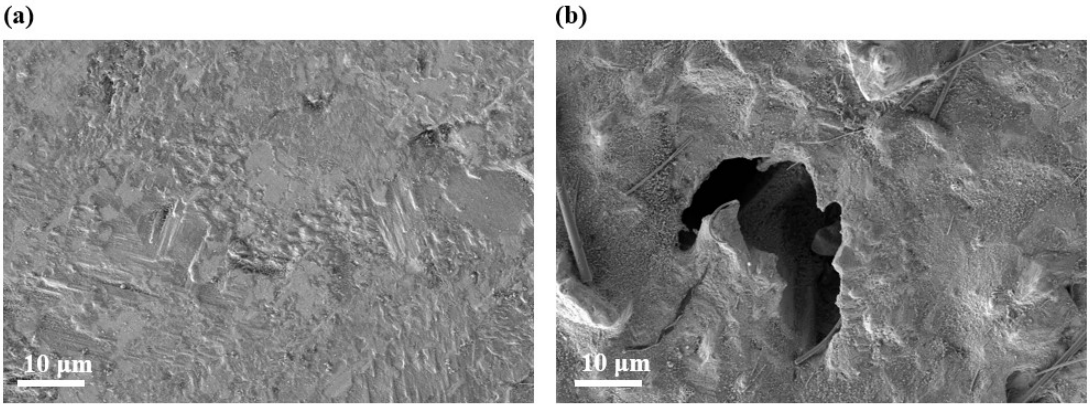

Fig. S19 SEM enlarged image of the surface of the recycled (a) FCL@Zn anode and (b) bare Zn anode.

Table S1. The performance comparison of Zn//Zn symmetric cells compared to previous reports.

Modification strategies	Current densities / Areal capacity (mA cm^{-2}/mAh cm^{-2})	Cycle performance (h)	Refs.
GFA-5	1/1	2000	[S1]
Zn-PA@Zn	5/2.5	1700	[S2]
ACG	20/5	2000	[S3]
Zn@ZSO	5/1	1500	[S4]
PPZ@Zn	1/0.5	3000	[S5]
Zn@CDs	1/1	3000	[S6]
E-nHAP@Zn	0.1/0.1	2400	[S7]
DX	5/5	1000	[S8]
ZnA@Zn	5/2	2400	[S9]
FCL@Zn	**5/2.5**	**3500**	**Our work**

Supplementary References

[S1] G. Liang, J. Zhu, B. Yan, Q. Li, A. Chen, Z. Chen, X. Wang, B. Xiong, J. Fan and J. Xu, *Energy Environ. Sci.*, 2022, **15**, 1086-1096.

[S2] H. Liu, J.-G. Wang, W. Hua, L. Ren, H. Sun, Z. Hou, Y. Huyan, Y. Cao, C. Wei and F. Kang, *Energy Environ. Sci.*, 2022, **15**, 1872-1881.

[S3] X. He, Y. Cui, Y. Qian, Y. Wu, H. Ling, H. Zhang, X.-Y. Kong, Y. Zhao, M. Xue and L. Jiang, *J. Am. Chem. Soc.*, 2022, **144**, 11168-11177.

[S4] R. Guo, X. Liu, F. Xia, Y. Jiang, H. Zhang, M. Huang, C. Niu, J. Wu, Y. Zhao and X. Wang, *Adv. Mater.*, 2022, **34**, 2202188.

[S5] X. Wang, J. Meng, X. Lin, Y. Yang, S. Zhou, Y. Wang and A. Pan, *Adv. Funct. Mater.*, 2021, **31**, 2106114.

[S6] H. Zhang, S. Li, L. Xu, R. Momen, W. Deng, J. Hu, G. Zou, H. Hou and X. Ji, *Adv. Energy Mater.*, 2022, **12**, 2200665.

[S7] K. Qi, W. Zhu, X. Zhang, M. Liu, H. Ao, X. Wu and Y. Zhu, *ACS Nano*, 2022, **16**, 9461-9471.

[S8] T. Wei, Y. Ren, Y. Wang, L. e. Mo, Z. Li, H. Zhang, L. Hu and G. Cao, *ACS Nano*, 2023, **17**, 3765-3775.

[S9] R. Zhao, J. Yang, X. Han, Y. Wang, Q. Ni, Z. Hu, C. Wu and Y. Bai, *Adv. Energy Mater.*, 2023, **13**, 2203542.